Transcriptional competition biases the effects of second messengers in *E. coli*

Andrea Ripamonti[1,2,§], Milan Lacassin[3,§], Rossana Droghetti[2], Gregory Bokinsky[3,+], and Marco Cosentino Lagomarsino[1,2,4,+,*]

[1]Dipartimento di Fisica, Università degli Studi di Milano, via Celoria 16, Milan, Italy
[2]IFOM Foundation, FIRC Institute for Molecular Oncology, via Adamello 16, Milan, Italy
[3]Department of Bionanoscience, Kavli Institute of Nanoscience, Delft University of Technology, Delft, The Netherlands
[4]INFN sezione di Milano, via Celoria 16, Milan, Italy
[§]These authors contributed equally
[+]These authors contributed equally
[*]Corresponding author: marco.cosentino-lagomarsino@ifom.eu

SUMMARY

Cells regulate gene expression by balancing transcriptional resources across different functional groups of genes. In bacteria, second messengers such as ppGpp and cAMP control ribosome biogenesis and metabolic gene expression, respectively. While these regulators are typically studied in isolation, we provide a theory showing that their effects are intertwined due to global transcriptional competition. Using experimental data from RelA overexpression and a mechanistic modeling framework, we show that ppGpp-mediated repression of ribosomal genes competes for transcriptional resources with cAMP-driven activation of metabolic genes. This competition reshapes proteome allocation in a way that transcends individual regulators. Our findings challenge classic assumptions about transcription factor action and suggest that large-scale gene regulation should be studied within the broader context of resource availability, with implications for understanding cellular regulation across diverse biological systems, beyond bacterial physiology.

KEYWORDS

bacteria, transcriptional regulation, ppGpp, cAMP, proteome allocation, ribosome, growth laws, nutrient sensing, RelA overexpression

INTRODUCTION

Precise regulation of gene expression is fundamental to cellular physiology, with implications for fitness and disease[1–4]. For instance, cells respond to growth limitations by expressing ribosomes and enzymes required to balance the supply and demand of key metabolites[5]. In this context, the proteome sector theory has emerged, particularly in bacteria[6–10], as a powerful mathematical approach that captures large-scale gene regulatory principles due to mass balance and supply-demand, including the well-established linear relationship between ribosomal content and growth rate (sometimes termed the "ribosomal growth law"[6,11]). Recent advances in proteomics have further refined our understanding of proteome allocation, revealing how cells can prioritize protein synthesis in response to environmental conditions and internal state[8,9,12–14].

A crucial open question is how cells integrate environmental signals and internal sensing to regulate ribosomal allocation and change the growth rate. One key mechanism for growth rate control in *E. coli* involves the alarmone (p)ppGpp (henceforth shortened as ppGpp), a global regulator of the ribosomal protein sector[1]. In conjunction with the transcription factor DksA, ppGpp binds to RNA polymerase (RNAP) inducing a conformational change that inhibits the transcription of genes encoding ribosomal RNA and proteins[15–18]. Additionally, ppGpp has many intracellular targets potentially linked to metabolism and translation, but the transcriptional effect appears to be dominant for ribosome regulation[15].

Recent work by Wu et al.[19] demonstrated that ppGpp levels quantitatively reflect translation elongation rates, establishing a direct link between the cellular perception of growth rate and ribosomal biogenesis. Mechanistically, ppGpp is synthesized from GTP by the ribosome-bound enzyme RelA when uncharged tRNAs bind to the ribosomal A site[20–22]. The enzyme SpoT also has a limited capacity for ppGpp synthesis, though its primary role is as a ppGpp hydrolase[23]. Thus, under starvation, ppGpp acts as a sensor of nutrient availability and redirects resources from the translation machinery towards metabolism[24,25].

Just as cellular resources must be efficiently allocated at the protein level, transcription itself requires careful distribution of RNA polymerase across different genes. The limited transcriptional capacity of the RNAP pool represents a fundamental constraint on gene expression, analogous to the limited proteome capacity[26–28]. This constraint means that increased transcription of one gene or set of genes necessarily affects the expression of others through competition for RNAP. While traditional views of transcriptional regulation focus on individual promoter-regulator interactions, the allocation of RNAP across different promoters emerges as a critical systems-level consideration, particularly when examining large-scale changes in gene expression such as those involving entire proteome sectors[29,30].

This perspective suggests that global regulators like ppGpp might coordinate cellular responses not only through direct promoter interactions but also by influencing the competition for RNAP allocation across the genome. Thus, their effect should depend on the contextual activity of other global regulators. One such example is the second messenger cyclic AMP (cAMP), a small molecule that modulates metabolic gene expression in response to the availability of carbon substrates[31,32]. Despite their distinct roles, both ppGpp and cAMP influence proteome allocation at the transcriptional level, shaping the ribosomal and metabolic sectors in response to nutrient availability.

Perturbing these second messengers by "opening the loops" of feedback control[33,34] provides a powerful means to test and refine our understanding of transcriptional regulation, offering key insights into regulatory interactions. For instance, Zhu and Dai[35] explored the effects of ppGpp overabundance by overexpressing its synthase enzyme, RelA, demonstrating that the ribosomal growth law is robust, despite broad proteomic rearrangements[36,37]. Similarly, Kochanowski and coworkers[38] showed that cAMP titration preserves the same growth law. While these find-

ings highlight the robustness of the ribosomal growth law, they also raise fundamental questions about the mechanisms governing proteome allocation under these perturbations. Intriguingly, prior studies suggest that the link between ppGpp and the growth rate is not univocal, particularly when RelA is overexpressed[39–41]. This divergence (reviewed in[42]) has so far remained unexplained and challenges the prevailing framework, suggesting a more complex interplay between ppGpp, global transcriptional regulation, and growth rate control.

Although recent models offer promising steps toward a mechanistic theory of proteome allocation, key gaps remain. Existing theories that connect proteome sectors with nutrient and growth sensing often overlook the mechanistic details of transcription[34,43,44]. Recent studies by Balakrishnan *et al.* and by Lin and Amir[26,30] provide a solid foundation for describing the flow of information from DNA to proteins, yet they are not fully embedded within the proteome sector framework. Conversely, the model proposed by Calabrese *et al.*[28] incorporates transcription and translation but lacks the regulatory details needed to capture the effects of second messengers.

In this work, we address the limitations of existing theories by adopting a theory-first approach. Building on the study of Balakrishnan *et al.*, we develop a framework that integrates transcriptional regulation by second messengers and competition for RNA polymerases into proteome sector models. This framework enables a model-guided analysis of experimental data. Leveraging published datasets from refs.[19,30,35–37,45], as well as performing new experiments involving RelA overexpression, we investigate a previously uncharacterized divergence in the relationship between ppGpp and ribosomal content. By simultaneously monitoring the levels of ppGpp and cAMP, we uncover non-trivial effects of second messengers on proteome coordination. These effects are effectively captured by our model, which describes second messenger–regulated transcriptional competition between proteome sectors.

RESULTS

Global transcriptional coupling connects differentially regulated proteome sectors

Building on the framework of Balakrishnan and coworkers[30], we introduce a model that integrates transcriptional regulation by second messengers and competition for RNA polymerases (RNAPs) into proteome sector dynamics (see Methods S1 for detailed derivations and assumptions). We denote the mass fraction of each proteome sector I as

$$\phi_I = \frac{M_I}{M} \ , \tag{1}$$

where M_I is the total mass of proteins in sector I and M is the total protein mass. For example, the "ribosomal sector" (ϕ_R) includes proteins involved in translation, while other sectors, such as metabolic (ϕ_P) and housekeeping (ϕ_Q), are categorized based on their response to growth limitations[6,8,9,32].

The model focuses on how mRNAs from different sectors are produced. We define the "transcriptome fraction" χ_I as the fractional proportion of mRNAs encoding proteins in sector I. Assuming no post-transcriptional regulation, the time evolution of protein mass fractions is given by (Methods S1 for derivation)

$$\frac{d\phi_I}{dt} = \epsilon f_a \phi_R \left(\chi_I - \phi_I\right) \ , \tag{2}$$

where ϵ is the translation elongation rate, f_a is the fraction of active ribosomes, and the product $\epsilon f_a \phi_R$ corresponds to the growth rate λ.

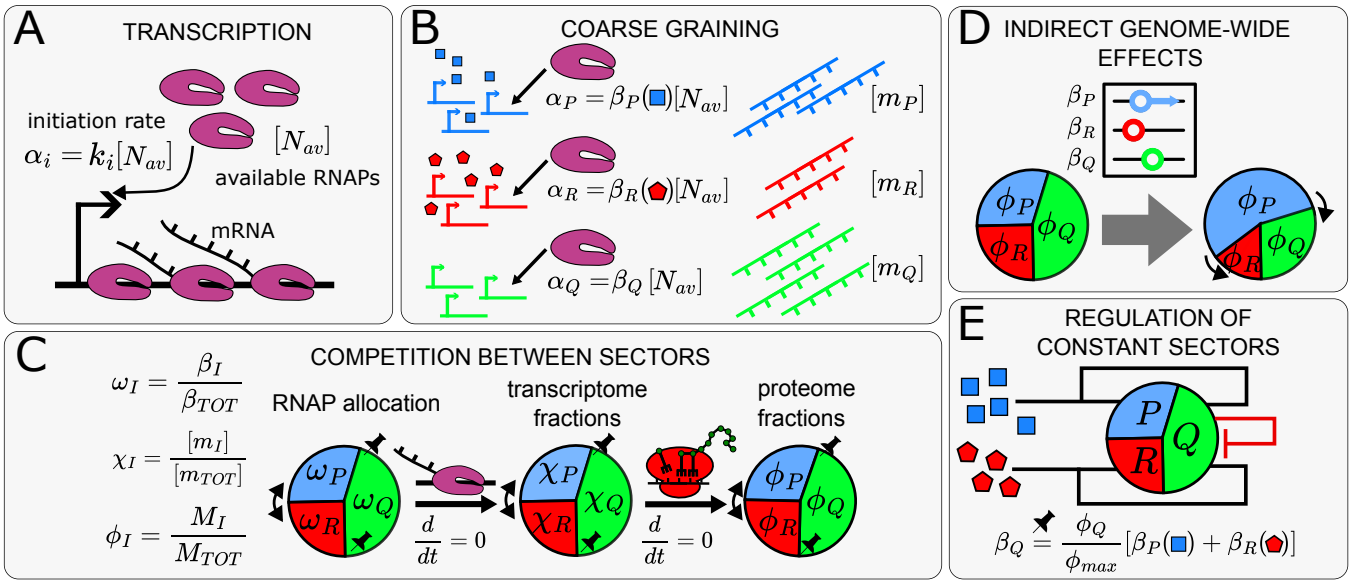

Figure 1: **Illustration of the model for transcriptional competition and its features.** (A) Transcription initiation rates are proportional to the concentration of available RNA polymerases $[N_{av}]$ (the model neglects traffic of RNA polymerase on genes). (B) Genes are grouped into sectors (three in this illustration). The R and P sectors are controlled by regulators, which act on the "sector strengths" β_R and β_P at the transcriptional level. mRNA abundances $[m_I]$ are determined by the coarse-grained initiation rates α_I. (C) Sector strengths determine the transcriptome fractions χ_I. The Q sector is assumed to be regulated in such a way that ϕ_Q is "pinned" at a constant value across conditions. At steady-state, transcriptome fractions correspond to proteome fractions ϕ_I. (D) Due to the normalization constraint, activation or repression of a single sector indirectly affects all others, even if their sector strengths remain unchanged. (E) Maintaining a constant Q sector size requires direct regulation, influenced either by signals coupled to the R and P sectors (black arrows) or by negative autoregulation (red T-shaped arrow), ensuring homeostasis.

Transcript dynamics are described in an "initiation-limited" regime[30,46], where the concentration of a transcript species $[m_i]$ evolves as

$$\frac{d[m_i]}{dt} = \alpha_i[G_i] - (\delta + \lambda)[m_i] \ . \tag{3}$$

Here α_i is the transcription initiation rate, δ is the uniform mRNA degradation rate and $[G_i]$ is the gene concentration. The dilution term $-\lambda[m_i]$ accounts for the time variation in cellular volume. Initiation rates depend on the concentration of available RNAP holoenzymes $[N_{av}]$, and are given by

$$\alpha_i = k_i[N_{av}] \ , \tag{4}$$

where k_i is the promoter strength, influenced by transcriptional regulators (see Methods S1 for details on initiation). Note that while it is possible to introduce a proteome sector for RNAP components to explore the system in different regimes of RNAP abundance[26–28], our framework does not rely on this description.

The key novelty of our approach lies in embedding transcription into proteome sector theory by introducing sector-specific coarse-grained promoter strengths β_I. This allows us to express mRNA dynamics at the sector level

$$\frac{d[m_I]}{dt} = \alpha_I[G] - (\delta + \lambda)[m_I] \ , \tag{5}$$

where we defined the "coarse-grained initiation rate" $\alpha_I = \beta_I[N_{av}]$ and the typical gene concentration $[G]$, which we assume to be uniform across all sectors (see STAR Methods and Methods S1 for a model variant including gene dosage effects). From this, we derive the time evolution of transcriptome fractions χ_I (Methods S1)

$$\frac{d\chi_I}{dt} = \frac{1}{\tau_\chi}(\omega_I - \chi_I) \ , \tag{6}$$

where $\omega_I = \frac{\beta_I}{\beta_{\text{TOT}}}$ represents RNAP allocation across sectors, with $\beta_{\text{TOT}} = \sum_J \beta_J$, while τ_χ is a characteristic relaxation timescale.

In steady-state growth, our model predicts that proteome fractions are determined transcriptionally by sector "strengths" as follows,

$$\phi_I = \chi_I = \omega_I = \frac{\beta_I}{\sum_J \beta_J} \ . \tag{7}$$

This relationship, proposed for single genes in ref.[30], implies that transcriptional regulation in one sector indirectly affects other sectors due to the normalization condition $\sum_I \omega_I = 1$ (Fig. 1D). This coupling is central to our framework, since it sets how global transcriptional regulation and competition for RNAPs shape proteome coordination.

Sectors with constant size must be actively maintained at a fixed expression level.

To understand the role played by transcriptional competition in setting the sizes of different sectors, we focused on a commonly used three-sector model[6,7,34] (see Discussion and Note S1 for details on four-sector models). This model typically assumes the mass fraction ϕ_Q of the housekeeping sector to remain constant[6]. We incorporate this constraint into our framework using Eq. (7) finding

$$\begin{aligned} \beta_Q &= \frac{\phi_Q}{\phi_{max}}(\beta_R + \beta_P) \\ \phi_R &= \frac{\beta_R}{\beta_P + \beta_R}\phi_{max}. \end{aligned} \tag{8}$$

Since sectors P and R are regulated in order to adapt to different conditions (e.g. different nutrients), the sum $\beta_P + \beta_R$ varies with the regulation, thus β_Q must follow its behaviour in a proportional way (Fig 1E). The second identity in Eq. (8) describes the competition between the P and R sectors for a proteome fraction equal to $\phi_{max} := 1 - \phi_Q$. Note that eq. (8) strictly applies only at steady-state. In addition, the first relationship does not necessarily imply that the Q sector shares transcriptional regulators with the other two sectors. For instance, some studies[6,29,47] have proposed that this sector maintains its constant size through negative autoregulation. Proteomics studies[8,9] indicate that Q consists of multiple subsectors (see Note S2 for details), each responding differently to growth limitations, while their overall sum remains constant. Regardless of the specific mechanisms governing Q, Eq. (8) provides the shape of its mean regulatory function in terms of β_P and β_R.

ppGpp and cAMP jointly coordinate proteome allocation by being linearly proportional to one another under catabolic limitation. With a constant Q sector, proteome allocation is entirely determined by the relative size of R and P from equation (8), and ppGpp is believed to be a central driver of this process[15,20,48] (Fig. 2A). To confirm this, we directly measured internal ppGpp levels in combination with growth rate across multiple conditions, corresponding to different carbon sources (see STAR Methods). We converted growth rate data into ribosomal fractions using the linear ribosomal growth law[6]. Consistent with the literature[19,35,39,49], we observed a robust relationship between ϕ_R and g, with elevated ppGpp levels corresponding to slower growth rates and thus smaller ribosomal fractions (Fig. 2B).

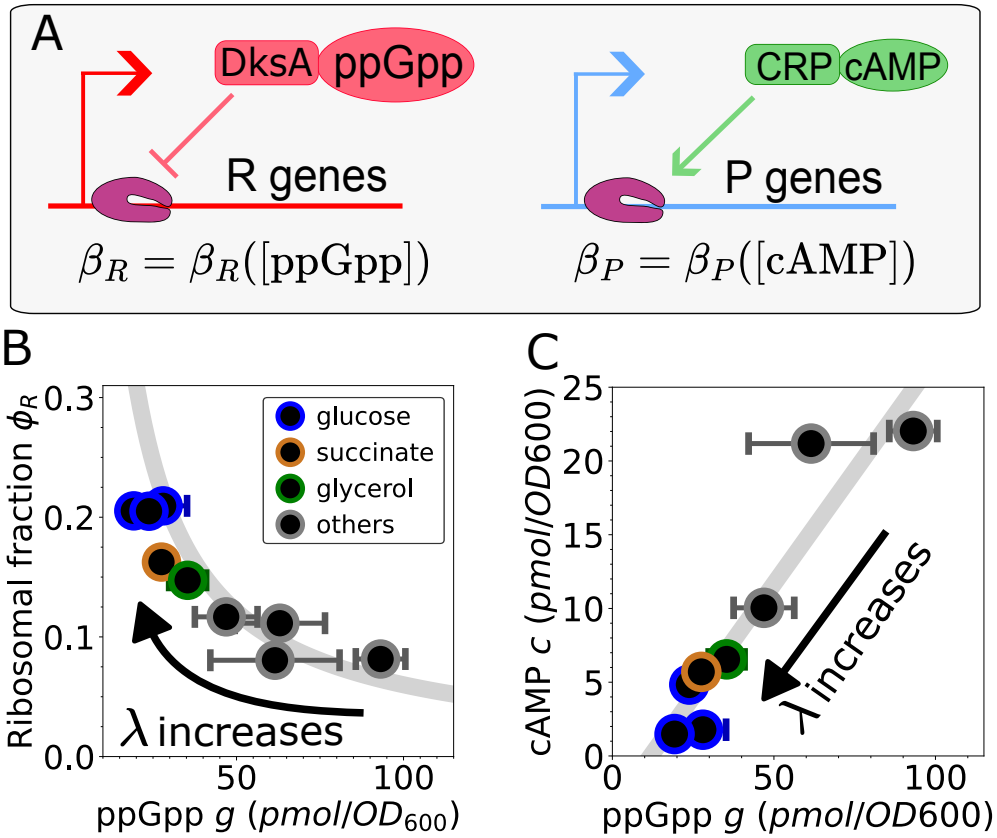

Figure 2: **A positive ppGpp-cAMP relation under catabolic limitation defines proteome allocation as a function of ppGpp.**(A) The model for transcriptional competition in *E.coli* can describe how the R sector is repressed by ppGpp-DksA, while the P sector is activated by cAMP-Crp. (B) Under catabolic limitation, the ribosomal fraction ϕ_R decreases with increasing ppGpp. The plot derives from our direct measurements of ppGpp levels and growth rate. Values for the ribosomal fraction are estimated from growth rate using joint measurements of RNA/protein ratio and growth rate from ref.[35]. The grey line represents the best fit according to the expression $\phi_R \propto \frac{1}{g}$ as in ref.[19]. (C) Under catabolic limitation, cAMP levels increase with increasing ppGpp (and therefore with decreasing growth rate) in a linear fashion (grey line, best fit) in the wild-type. This correlation obscures the specific effect of cAMP on ϕ_R when considered solely as a function of ppGpp.

With only three proteome sectors, incorporating a passive P sector is sufficient to account for this growth rate-dependent proteome partitioning, consistently with the original suggestion by Scott and coworkers[6]. Under these assumptions, proteome composition at equilibrium is a function of ppGpp only: $\phi_R = \phi_R(g)$ and $\phi_P = \phi_P(g)$. Models with ppGpp as the sole transcriptional regulator are commonly found in the literature[19,34,43], because this minimal setup effectively captures the correlation between ϕ_R and g across nutrient conditions seen in various *E. coli* studies.

However, previous studies[1,32,38,50–52] show the importance of the second messenger cyclic AMP (cAMP) as a global regulator. cAMP activates the transcription factor CRP (cAMP receptor protein), which in turn drives catabolic gene expression by binding specific DNA sequences and interacting with the α subunit of RNA polymerase[31,53,54]. Produced by adenylate cyclase (Cya), cAMP levels depend on carbon substrate availability. You *et al.*[32] proposed that Cya activity is repressed by alpha-ketoacids (e.g., oxaloacetate), forming a feedback loop: when alpha-ketoacids accumulate, cAMP synthesis and catabolic gene expression are downregulated, allowing *E. coli* to adjust its metabolism according to nutrient availability.

Catabolic proteins are part of the metabolic sector, along with the anabolic ones[1,32]. The anabolic sector can be considered passive as a first approximation[38]. Hence, we can describe the metabolic sector strength β_P as a function of cAMP concentration c, $\beta_P = \beta_P(c)$ (Fig. 2A), while for the R sector we can set $\beta_R = \beta_R(g)$. Thanks to Eq. (8) we can write, at steady state,

$$\phi_R(g,c) = \frac{\beta_R(g)}{\beta_R(g) + \beta_P(c)}\phi_{max} = \left[1 + \frac{\beta_P(c)}{\beta_R(g)}\right]^{-1} \phi_{max} \ . \tag{9}$$

Crucially, ϕ_R becomes a function of both ppGpp and cAMP concentrations. The strong variation of ϕ_R with g in wild-type data can be explained in two ways: either cAMP signaling plays a minor role compared to ppGpp regulation, or cAMP levels vary jointly with ppGpp as a function of growth rate, $c = c(g)$. To distinguish between these scenarios, we measured cAMP levels under the same conditions as in Fig.2B using the same methodology as for ppGpp. Consistent with the second hypothesis, we observed that ppGpp and cAMP levels covary linearly (Fig.2C). As ppGpp levels increase, repressing the R sector, cAMP concentrations rise concurrently, activating the P sector. This coordinated response ensures that both cAMP and ppGpp collectively redirect resources from translation to metabolism, reflecting a joint modulation of proteome allocation by these second messengers.

We refer to the Discussion for further details and hypotheses on the coordination between cAMP and ppGpp. This positive correlation is observed specifically under catabolic limitation, where growth is restricted by changing the carbon source. However, we predict different behaviors to emerge under other perturbations (SI Note 1). An important example is titration of the enzyme glutamate synthase (anabolic limitation), where cAMP levels are known to decrease with decreasing growth rate, and the ribosomal growth law is conserved[32,38]. Since downregulation of ribosomes with decreasing growth rate requires increasing ppGpp, we predict ppGpp and cAMP to be anticorrelated under anabolic limitation. Specifically, if this perturbation starts from a point on the wild-type curve in Fig. 2B, the system will explore the region of the ppGpp-cAMP plane below the wild-type curve (Fig. S5).

RelA overexpression reveals indirect regulation of ribosomal proteins by transcriptional competition with cAMP targets.

Having established that ppGpp and cAMP are linearly correlated under catabolic limitation, we reasoned that perturbations in ppGpp levels could disentangle this correlation and reveal the effects of transcriptional competition. To test this, we titrated ppGpp by overexpressing the N-terminal catalytic domain of the enzyme RelA (referred to as RelA*) using an inducible TetR-pTet system. We measured steady-state growth rate together with ppGpp and cAMP concentrations at different degrees of induction, and with different carbon sources as supplements (see STAR Methods).

Previous studies have explored RelA* overexpression and provided key insights that inform our analysis. Firstly, this perturbation is known to reduce the steady-state growth rate[35,39,55], a finding confirmed in our data (Fig. S1A). As mentioned in the Introduction, Zhu and Dai.[35] demonstrated that this decrease in growth rate is also associated with a reduction in rRNA content (a proxy for the ribosomal fraction[6]), while the relationship between the two (the ribosomal growth law) remains unchanged (Fig. S2A). Thanks to this observation, we are able to convert growth rates into ribosomal fractions with the same coefficients used for the unperturbed conditions (STAR Methods).

As mentioned in the Introduction, previous studies have suggested that the relationship between growth rate λ and ppGpp g breaks under RelA overexpression, therefore the relationship between the ribosomal sector and ppGpp, which is central to wild-type physiology (Fig. 2B), must also be broken. This is noteworthy, as one might expect that elevating ppGpp levels in RelA overexpression mutants would simply shift cells to a slower growth regime, while still maintaining the

wild-type $g - \phi_R$ correlation. However, our measurements confirm that the relationship between ϕ_R and g is not conserved (Fig. 3A).

Specifically, at equivalent ppGpp concentrations, RelA* overexpression mutants, despite an overall decrease in their growth, displayed higher growth rates, and hence higher ribosomal fractions, compared to the wild-type (Fig. 3A and Fig. S1A). In other words, RelA* overexpression reduces the repressive power of ppGpp on ribosome biogenesis, as the same levels of ppGpp give higher ribosomal levels compared to the unperturbed condition. Similarly, this conclusion is supported by comparing recent data from refs.[36,37] with our wild-type data (Fig. S2C).

Therefore, our observations support the idea that ribosomal content is not solely dependent on ppGpp levels. This challenges regulatory models that propose ppGpp as the exclusive regulator of proteome partitioning. Instead, our findings support a more complex scenario involving competition for RNA polymerase between multiple large-scale gene expression programs, described by our model through Eq. (9).

To further explore this deviation, we examined the relation between ppGpp and cAMP under RelA overexpression. Remarkably, cAMP concentration data points fall below, rather than on, the wild-type ppGpp-cAMP curve (Fig 3B). This implies that, at the same ppGpp concentration, the P sector is less activated by cAMP compared to the physiological level of activation found in the wild-type strain. The trend in cAMP data is in line with a constant for growth in minimal medium supplemented with glucose (blue arrow), and is compatible with a constant for minimal medium supplemented with succinate (ochre arrow). For these two conditions, we can reasonably conclude that cAMP levels remain largely unaffected by RelA overexpression. The behavior observed in glycerol is more complex, yet cAMP levels still remain below the wild-type curve (gray line).

Based on these observations, we determined the functional shapes of the two sector strengths β_P and β_R required for the model to reproduce our data for both wild-type and and RelA* overexpression mutants. Using Eq. (9), we found that a model with

$$\begin{aligned} \beta_P(c) &= \rho \left[\mu_1 \left(1 + \frac{c}{\mu_2} \right) \right] \\ \beta_R(g) &= \rho \left[1 + \frac{\mu_3}{g} \right] \end{aligned} \tag{10}$$

reproduces the data well (see Fig. S3A for an estimate of the goodness of fit), where μ_1, μ_2, μ_3 can be fixed by fitting (Table S1) and ρ remains a free parameter. The predictions of the model can be visualized as a function of ppGpp by assuming a relationship between cAMP and ppGpp for each carbon source. Fig. 3A shows the outcome assuming the best linear fits, represented by arrows in Fig. 3B. Other representations of the cAMP-ppGpp relationship lead to slightly different visualization in the $g - \phi_R$ plane (Fig. S3B,C) without impacting the quality of the fit.

While this model is fairly rich in parameters, it gives rise to simple interpretations. The parameters μ_2 and μ_3 are, respectively, effective cAMP and ppGpp concentrations. The parameter μ_1 accounts for different number of genes and basal promoter strengths between the two sectors. A basal rate for the R sector is necessary because extreme ppGpp overabundance does not reduce the ribosomal fraction to the lowest levels observed in the wild type; instead, ϕ_R appears to approach an asymptotic value, particularly for glucose and glycerol (Fig 3A, high ppGpp region). The basal rate for the P reflects the contribution from its anabolic subsector[38] (see Discussion and Supplemental Note 1 for details).

The model also necessarily includes the free parameter ρ, because our approach is only able to access the *ratio* $\frac{\beta_P}{\beta_R}$ (see Eq. (9)). Therefore, the model is invariant with respect to scaling both activities by a common multiplicative factor, which potentially keeps into account transcriptional effects shared by the two sectors, as well as potential influence of ppGpp on Crp activity[56]

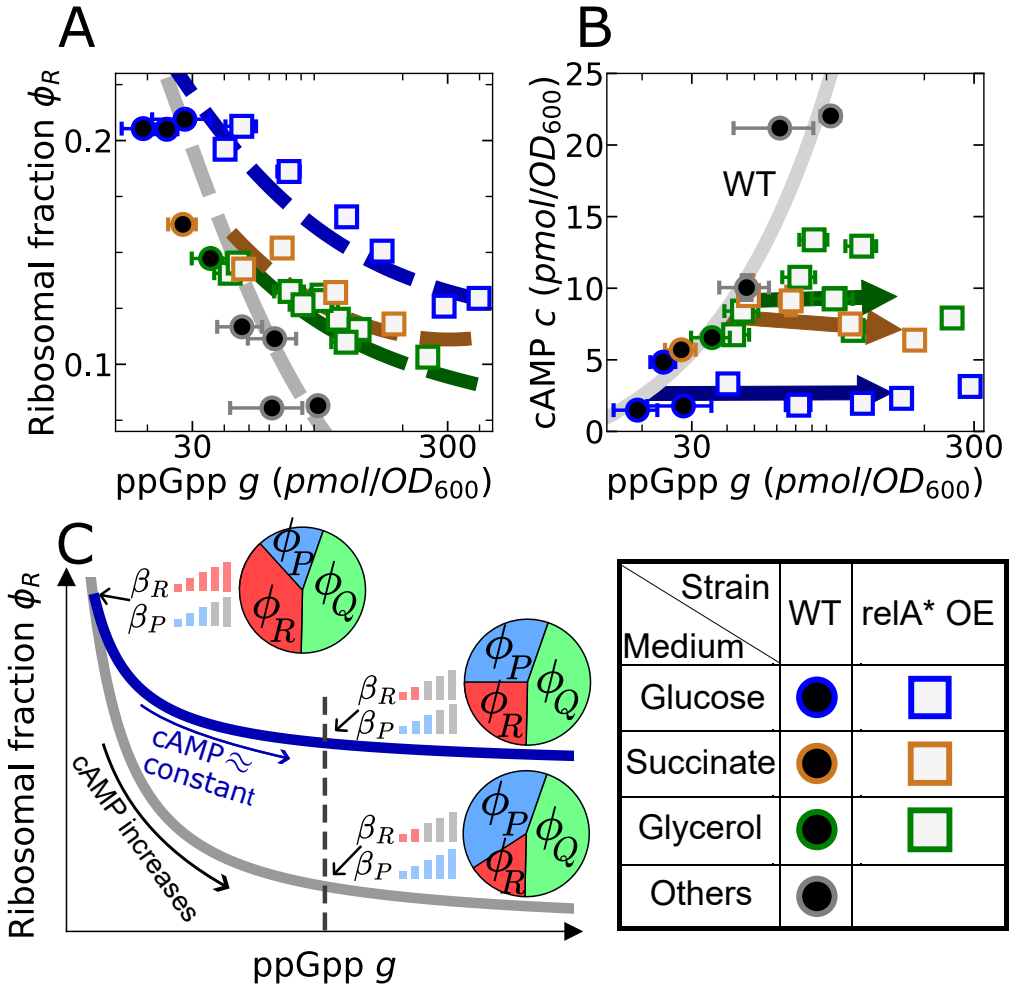

Figure 3: **Under RelA overexpression, transcriptional competition with cAMP-activated genes decreases ppGpp-mediated repression, falsifying models that neglect resource competition.** (A) Upon RelA overexpression (squares), the wild-type relation between ϕ_R and ppGpp (circles) breaks down. By a proper choice of the functions $\beta_R(g)$ and $\beta_P(c)$, the model reproduces both wild-type (gray dashed line) and RelA overexpression data (colored dashed lines). To visualize the model's predictions, we assumed that cAMP levels vary linearly with ppGpp changes during RelA overexpression (see STAR Methods), as indicated by the arrows in Fig 3B. B) The WT relation between ppGpp and cAMP (solid grey line, same as in Fig. 2C, but in log scale) is broken when over-expressing RelA. For a fixed carbon source, cAMP levels vary only minimally with increasing ppGpp. Arrows indicate the linear fits used as input for the model predictions in panel A. (C) Origin of the branching in Fig. 2A. At low ppGpp, ribosomal promoters operate at maximal capacity, while the P sector is minimally activated. If RelA is overexpressed starting from this condition (blue line), R is repressed by the increased ppGpp concentration, but the intrinsic activation of the P sector remains approximately constant due to unchanged cAMP levels. Conversely, if the same ppGpp concentration is achieved in the wild-type by worsening the nutrient quality (black line), cAMP levels rise and activate the P sector. This results in a smaller ribosomal fraction in the latter case.

(Discussion and Methods S1). For simplicity, we assume the absence of such effects, treating ρ as a constant. However, even if these effects were present, we note that ρ would only affect the total promoter strength β_{TOT}, without influencing competition between the R and P sectors, which is fully determined by the effective concentrations μ_2 and μ_3.

We can illustrate the key features of the model using glucose as a reference condition (Fig. 3C). In wild-type cells growing on glucose, ppGpp and cAMP levels are low: this leads to strong derepression of the R sector, with a lack of activation of the P sector, resulting in a high ribosomal fraction. When ppGpp increases due to RelA overexpression (blue line in Fig. 3C) while keeping glucose as the carbon source, it represses the R sector. However, because cAMP levels remain constant, the P sector is not activated, leading to only a small reduction in ϕ_R. In contrast, when ppGpp increases to the same value due to worsened nutrient quality (black line in Fig. 3C), cAMP levels rise in tandem activating the P sector and resulting in a more significant downregulation of the ribosomal sector. Note that this reasoning also applies when cAMP levels are not constant under RelA overexpression, as long as they remain below the wild-type cAMP-ppGpp curve, as seen in glycerol (green squares in Fig. 3B).

Thus, the relationship between ppGpp and R sector expression observed in wild-type conditions is not only a consequence of ppGpp repression but also a result of transcriptional competition (or equivalently a competition for allocation of free RNA polymerase) with the P sector, which is activated by cAMP. In contrast, during RelA* overexpression, the relationship between ppGpp and R sector expression reflects ppGpp repression alone, without competition from the P sector. Consequently, repression of the ribosomal sector appears weaker in this condition, as higher ppGpp levels are required to suppress ribosomal protein expression compared to wild-type conditions.

This is the central result of our study: R sector expression is determined not only by ppGpp concentrations but also by constraints imposed by RNA polymerase allocation and transcriptional competition with other sectors.

Alternative explanatory models require transcriptional competition between sectors. To assess the robustness of our findings, we explored various alternative models to account for potential confounding factors that could contribute to the observed data. One such factor is gene dose-dependent effects, which are not explicitly included in the simplest version of our framework. While we present a method to address these in the Methods S1 document, we briefly note here that the growth rate dependence of the ori/ter ratio, which determines copy numbers, remains unchanged under ppGpp overabundance[57]. Building on this, we show that gene copy number variations do not account for the divergence in the relationship between ϕ_R and g (Methods S1). Within the examined growth rate range, these effects are minimal, and incorporating them into our fitting algorithm results only in parameter adjustments (Table 1). Moreover, we note that the branching in Fig. 3A is not caused by variations in the rate of replication initiation, which may be under complex regulation[57]. This is because our definition of regulatory functions is independent of Ori concentration, which influences total gene concentrations, but not relative levels. Additionally, it is important to emphasize that our model is independent of the speed of transcriptional elongation or cell size, variables that are both known to be affected by RelA overexpression[49,55], but are not related to transcriptional competition.

In addition, considering the mechanisms of ppGpp-dependent repression of ribosomal genes, attention should be given to the role of DksA, which is required for ppGpp activity as a transcriptional repressor of the ribosomal sector. One might propose that ppGpp-mediated repression becomes limited by DksA under high ppGpp levels. However, data from refs.[9,58] show that, in the wild-type, DksA is maintained at a constant level across perturbations, which likely reflects negative autoregulation of its gene[59]. Therefore, we can safely exclude the possibility of a DksA-limited regime, particularly for ppGpp values in the typical wild-type range, where branching is already recorded (Fig. 3A). Indeed, existing observations report consistently high concentrations

of DksA across various conditions[17]. Incidentally, the proteomics data from ref.[9] report that the abundance of Crp, which is essential for cAMP signaling, increases under catabolic limitation in the wild-type. This increase can be interpreted as an adaptation to the cellular levels of cAMP, supporting frameworks like ours[32], where cAMP functions as a sole regulator, without explicitly considering Crp. Refined models where a Crp-cAMP regulator is limited by Crp are possible, but these details appear to go beyond the question of transcriptional competition.

In principle, other scenarios can be conceived to describe our data. For instance, one might consider allowing ϕ_Q to vary, leading to various model configurations. We demonstrate that a model where the sector strength β_Q remains unchanged during RelA overexpression, while the P sector is treated as passive, fails to explain the observed data. This alternative model predicts a greater downregulation of the R sector compared to wild-type conditions, which contradicts our findings (Methods S1 for proof). As a second alternative, we explored a model where, under RelA overexpression, proteome resources released by the R sector are allocated to the Q sector, while ϕ_P remains constant. Within our framework, we demonstrate that cAMP-mediated activation of the P sector is still necessary in this scenario (Methods S1).

Thus, we conclude that, within the range of scenarios we considered, transcriptional competition is a necessary ingredient for the model to reproduce the behavior of our experimental data shown in Fig. 3A.

Suboptimal proteome allocation is maintained by distorted sensing of elongation rates. The observation that the $\phi_R - \lambda$ relationship is conserved under RelA overexpression, while the $\phi_R - g$ relationship is not, prompted us to investigate the behavior of other variables of the system in relation to ppGpp. Specifically, we focused on the relation between translation elongation rate ϵ and g. Wu and coworkers[19] reported a solid link in the wild type between these two variables, even under out-of-steady-state conditions (Fig. 4A), as follows

$$\frac{g}{g_0} = \frac{\epsilon_{max}}{\epsilon} - 1 \ , \tag{11}$$

where ϵ_{max} represents the maximal elongation rate, and g_0 denotes a reference ppGpp concentration. It has also been reported that the $\epsilon - \phi_R$ (and hence $\epsilon - \lambda$) relationship remains substantially unchanged under RelA* expression[35] (Fig. S2B); therefore, ppGpp overexpression cannot preserve the relationship established by Eq. (11).

Fig. 4 explicitly shows this point using the data in ref.[35] to convert growth rate data from our experiments into elongation rate values (STAR Methods) and plot them against ppGpp concentration. As expected, Fig. 4B shows that RelA overexpression breaks Eq. (11). In fact, at equivalent elongation rates, we find higher ppGpp concentrations in RelA* overexpression mutants. This change can be described as a distorted sensing of elongation rates by the cell[19]. At equivalent values of ϵ, cells perceive harsher conditions than those actually present. It is important to note that if the cAMP-ppGpp linear relation (Fig. 2C) were conserved upon RelA* overexpression, our model would predict a collapse on the wild-type curve for ϕ_R as a function of ppGpp, despite distorted sensing of ϵ. Thus, distorted elongation rate sensing, combined with disrupted cAMP-ppGpp coordination, acts to maintain suboptimal proteome allocation when RelA is overexpressed.

We also note that this prediction is compatible with the theory proposed by Wu and coworkers[19] for the wild-type. Here, the steady-state ppGpp concentration is given by the equilibrium between synthesis by RelA, with rate a, and hydrolysis by SpoT, with first-order rate constant b, yielding $\frac{g^{eq}}{g_0} = \frac{a}{b}$. The synthesis rate is proposed to be proportional to the number of "dwelling" ribosomes, and the hydrolysis rate to be proportional to the number of ribosomes in the translocating state of elongation, so that the ratio $\frac{a}{b}$ becomes a function of the elongation rate, $\frac{a}{b} = \frac{\epsilon_{max}}{\epsilon} - 1$, leading to (11).

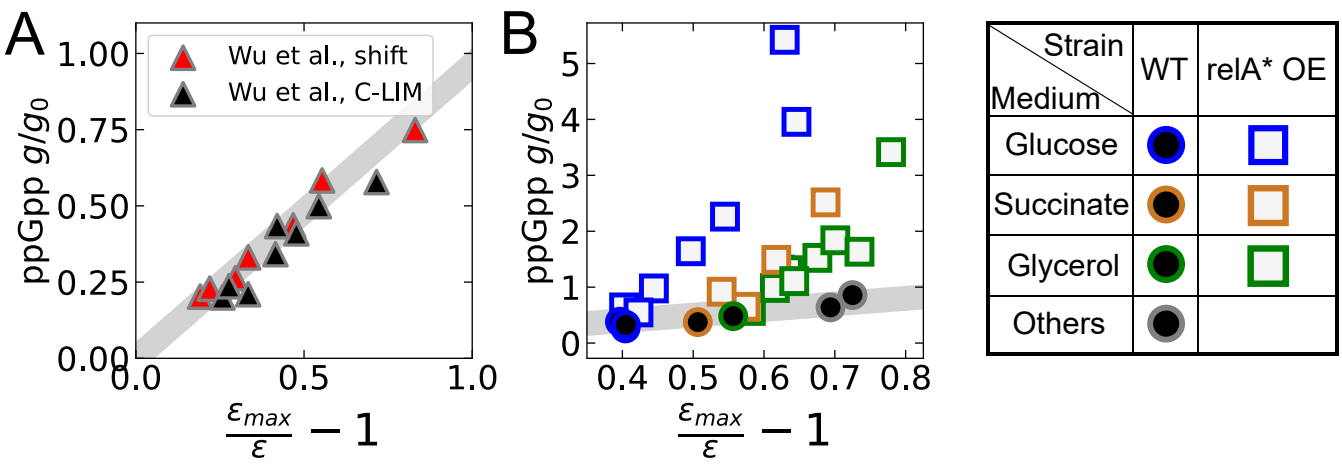

Figure 4: **RelA* overexpression causes distorted sensing of elongation rates.** A) In the wild-type, ppGpp levels are determined by the elongation rate thanks to sensing by RelA, leading to (11). Data from ref.[19] for a diauxic shift (triangles) or catabolic limitation (squares). B) ppGpp levels vs elongation rates as calculated from our growth rate data, using the elongation rate growth law in ref.[35]. Our estimates show that the linear wild-type relation in panel A does not hold under RelA* overexpression. At the same elongation rate ϵ, ppGpp is more abundant in RelA* overexpression mutants, reflecting the excess of synthase domains and the lack of compensation by SpoT. For both panel A and panel B, gray lines represent the best linear fit of wild-type data according to (11), with $g_0 \approx 70\ pmol/OD_{600}$ for our data.

Assuming this theory, we can explain ppGpp overabundance in Fig. 4 as follows. In our RelA overexpression strain, ppGpp synthesis is also carried out by the truncated RelA enzyme, which has constitutive activity[39,60]. We write ppGpp dynamics and its equilibrium concentration as follows

$$\begin{aligned} \frac{1}{g_0}\frac{dg}{dt} &= a + k_* - bg \\ \frac{g^{eq}}{g_0} &= \frac{a+k_*}{b} > \frac{\epsilon_{max}}{\epsilon} - 1 \end{aligned} \tag{12}$$

Here k_* represents the constitutive synthase activity of RelA*, which varies with the degree of induction. Consistent with this, we compute k_* from our data and demonstrate its correlation with the concentration of the pTet inducer, doxycycline (Methods S1). As a result, for the same elongation rate ϵ (i.e., for the same number of dwelling and translocating ribosomes), RelA* induction corresponds to increased ppGpp.

We must also note that if we focus on a single carbon source, not only is ppGpp concentration higher than in the unperturbed condition, but ϵ also decreases ($\frac{\epsilon_{max}}{\epsilon} - 1$ increases). We attribute this change to the feedback loop between ppGpp and the translation apparatus[34,44]. We expect increasing ppGpp through RelA overexpression and keeping the nutrient source fixed leads to transcriptional repression of tRNAs and translation factors, which are co-regulated with ribosomes. According to the theory by Dai et al.[45], this would in turn cause ϵ to decrease.

Transcriptional regulation of hibernation factors explains deviations in ribosome inactivity.

In addition to elongation rate ϵ and ribosome proteome fraction ϕ_R, the fraction of actively translating ribosomes, f_a, is a crucial determinant of growth rate[45]. We can calculate f_a using the relationship $f_a = \frac{\lambda}{\epsilon\phi_R}$. This definition assumes negligible protein degradation, which plays a role in setting the fraction of active ribosomes, particularly at very low growth rates[46]. In the

following, we maintain this simplifying assumption, as it provides a reasonable approximation in moderate-to-fast growth conditions[34,46].

The primary contribution to inactive ribosomes is generally attributed to ribosome deactivation by hibernation factors[19]. Other factors, such as stalled ribosomes[45] and mRNA scarcity[28] might also play a role, but we focus for simplicity on inactivation by hibernation factors, following the model proposed in ref.[19]. In *E. coli*, four main hibernation factors, Rmf, RaiA, RsfS, and Hpf, dimerize or sequester ribosomes and their subunits[61–63], thereby preventing them from initiating translation. We group these factors into a new sector characterized by a mass fraction ϕ_{HIB} and assume complete binding of hibernation factors to ribosomes, expressed as

$$\phi_{HIB} \propto \phi_R^{in} = (1 - f_a)\phi_R \ , \tag{13}$$

again in line with Wu *et al.*[19]. Here ϕ_R^{in} is the mass fraction associated with the inactive ribosomal sector.

Knowledge of λ and the values of ϕ_R and ϵ allow us to calculate f_a and ϕ_R^{in} in our data and plot them against ppGpp concentration (Fig 5A and 5B). Our results reveal a significant deviation from the wild-type relationship: at equivalent ppGpp concentrations, RelA overexpression mutants display higher values of the active fraction f_a, despite an overall decrease with overexpression. This suggests that ϕ_{HIB} is not regulated exclusively by ppGpp, as proposed in the model of ref.[19].

We speculated that this fact might also be a consequence of transcriptional competition. To explore this possibility, we introduce a collective promoter strength associated with hibernation factors, β_{HIB}. Fig. 5C provides a schematic representation of how second messengers could be influencing this variable in relation with the mass fraction ϕ_{HIB}, taking again glucose as a reference. At the same ppGpp concentration g_{AB}, wild-types (point A) present a higher cAMP concentration with respect to RelA overexpression mutants (point B), i.e., $c_A > c_B$. Our data indicate that $\phi_{HIB}(B) > \phi_{HIB}(A)$, which at steady-state can be written in terms of promoter strengths from (7) (STAR methods for derivation)

$$\frac{\beta_{HIB}(A)}{\beta_R(g_{AB}) + \beta_P(c_A)}\phi_{max} > \frac{\beta_{HIB}(B)}{\beta_R(g_{AB}) + \beta_P(c_B)}\phi_{max} \ . \tag{14}$$

This inequality captures the competition between the hibernation sector in the numerators and the P and R sectors in the denominators. Since the denominator is greater for the wild-type (left-hand side) due to the activation of the P sector by cAMP, the inequality suggests that the strength of the hibernation sector must also be higher in wild-type cells, i.e., $\beta_{HIB}(A) > \beta_{HIB}(B)$.

This model shows that the data are consistent with cAMP activating the hibernation sector, in addition with the reported effect by ppGpp[19]. Notably, here the deviation from the wild-type line arises from a regulatory effect, rather than simply from competition for RNA polymerase, as was observed for the ribosomal fraction ϕ_R (Fig. 3C). Indeed, global coupling acts on the denominator, and taken alone it would cause the opposite relationship: $\phi_{HIB}(A) < \phi_{HIB}(B)$ due to activation of the P sector by cAMP, with $\beta_P(c_A) > \beta_P(c_B)$. Therefore, we hypothesize that cAMP may regulate a direct transcriptional activation of the hibernation sector. In line with this claim, cAMP was found to activate the genes for both Rmf and RaiA[63,64].

This transcriptional model for hibernation factors may also explain why the ribosomal growth law $\phi_R(\lambda)$ remains the same of the wild-type under anabolic limitation[32,38] and in the "cAMP titration" strain examined in ref.[38]. Its conservation suggests that both ϵ and f_a must are able to adjust to ribosomal abundance across these perturbations, which we predict to break the ppGpp-cAMP relationship seen under catabolic limitation (Fig. 2C). Indeed, we expect the region of the ppGpp-cAMP plane explored under RelA overexpression to overlap with that typical of anabolic limitation (Fig. S5).

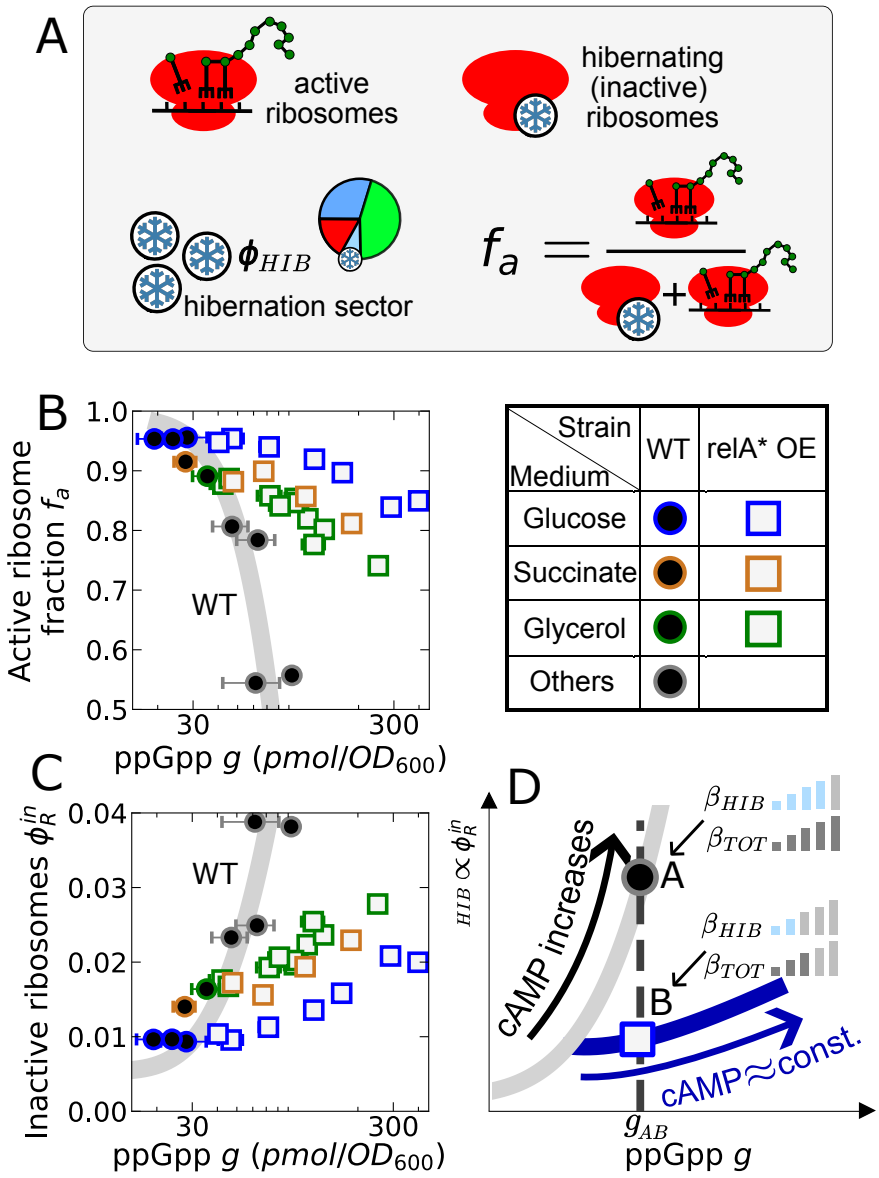

Figure 5: **Transcriptional activation of hibernation factors by cAMP explains deviations in the fraction of active ribosomes.** (A) Scheme of the model. We consider two populations of ribosomes: actively elongating ribosomes (with fraction f_a), which contribute to translation and growth, and hibernating (inactive) ribosomes. A proteome sector containing the hibernation factors, has mass fraction ϕ_{HIB}. (B) Estimates for the fraction of active ribosomes $f_a := \frac{\lambda}{\epsilon\phi_R}$, calculated from our growth rate data, plotted against ppGpp. The grey line is obtained with this definition, using the wild-type growth laws for ϵ and ϕ_R as in ref.[45] and ref.[35] (see STAR Methods). Under RelA overexpression, f_a decreases as a function of ppGpp, but its decrease is less pronounced with respect to unperturbed data. (C) Under RelA overexpression, the estimated proteome fraction corresponding to inactive ribosomes ϕ_R^{in} increases more gradually with ppGpp. The grey wild-type line is obtained analogously to the one in panel A, through equation (13) (STAR Methods).(D) Results in panel B can be explained by a transcriptional competition theory where hibernation factors are activated by both ppGpp and cAMP, with a strength β_{HIB}, explaining their scarcity under RelA overexpression.

DISCUSSION

The primary result of our combined approach integrating coarse-grained modeling and data is that allocation of RNA polymerase towards catabolic genes decreases expression of ribosomal genes. This is a form of indirect repression that requires no direct regulatory interactions between Crp and cAMP with ribosomal promoters. Instead, cAMP acts by inducing the expression of catabolic genes, which compete for transcriptional resources (primarily RNA polymerase) with the ribosomal sector for proteome allocation (Fig. 3C). While there is a large body of work on how different regulators control the various components of the proteome[19,32,38,54], the impact of these regulatory circuits on the global scale is relatively unexplored[1,30,38,65,66]. In bacteria, the prevailing consensus sees ppGpp alone as a governor ribosome allocation, overriding the influence of other regulators[15,54]. However, data collected in this study confirm the previous observation[39,40,42] that ribosome allocation is not solely dependent on ppGpp outside physiological conditions. Indeed, capacity of ppGpp to repress expression of ribosomes is decreased under RelA overexpression (Fig. 3A).

The linear relation observed between cAMP and ppGpp under catabolic limitation in the wild-type strain is consistent with theoretical predictions by Erickson et al.[50] and Scott and Hwa[1]. These authors propose that coordination between ppGpp and cAMP in the wild-type arises from a mechanistic link between the two signals, possibly due to their sensitivity to ketoacids and amino acids, which are coupled via transamination. Under this framework, the disruption of coordination observed under RelA overexpression could be attributed to ppGpp's distorted sensing of the elongation rate and, consequently, of the amino acid pool. Alternatively, the correlation might be non-causal, simply reflecting the shared role of ppGpp and cAMP as stress signals under catabolic limitation. Since we cannot distinguish between these causal and non-causal explanations, we leave this question open for future investigation.

Our theory places cAMP on par with ppGpp as "orthogonal" signals: not only do they control different parts of the proteome, but their levels must also be independently adjusted, since we observed deviations from the wild-type ppGpp-cAMP correlation under RelA overexpression (Fig. 3B). However, some interactions have been reported, ranging from ppGpp-induced induced acetylation of Crp[67] and direct binding of ppGpp to Crp, which can impair its activity[56,68]. These non-orthogonal effects can be included in the ρ factor in (9), without substantial changes to the model (Methods S1).

We note that the ketoacids-amino acid coupling would be dependent on anabolic enzymes in the "A sector"[1,32], for which a coarse-grained regulatory theory is still not well-defined[1]. The A sector has been proposed to be passive (constitutive)[38], and we initially approximated it as such in our model. However, we observe that the downregulation of the A sector under catabolic limitation in the wild-type[9] cannot be explained by constitutive-like behavior (Supplemental Note 1), which is characterized by the opposite trend. We also note that, while some works reported activation of anabolic promoters by ppGpp[18], this mechanism alone would again result in the incorrect regulation. To demonstrate that our model remains valid regardless of this approximation, we have attempted a more data-driven approach in defining the sector that competes with ribosomes, using gene targets of cAMP as cataloged in databases such as RegulonDB[69] and EcoCyc[70] (consulted February 2025), rather than relying on phenomenological definitions of proteome sectors. Our analysis revealed that cAMP-activated genes are distributed across the entire proteome, including the Q sector (Fig. S4A,B). As a result, ribosomal proteins may be considered in competition for RNA polymerase with a "cAMP-activated sector" that does not perfectly overlap with catabolic proteins. This variant adequately describes the data, requiring only a modification of parameters (Table 1 and Supplemental Note 2).

The remarkably robust conservation of the ribosomal growth law $\phi_R(\lambda)$ under both ppGpp

and cAMP perturbation[35,38] under lack of coupling between ppGpp and cAMP requires an explanation. To maintain consistency, we showed that the fraction of active ribosomes f_a must not depend solely on ppGpp. Our analysis shows that a theory of transcriptional regulation of ribosome-hibernating factors can capture this behaviour. Specifically, we speculate that activation of the hibernation sector by cAMP could be one of the factors contributing to this observation, thereby recreating the growth law. While there is evidence of a role of cAMP in regulating this sector[63,64], additional studies on this point are required, as hibernation factors could also be regulated post-transcriptionally (raiA and rmf in ref.[71]), or additional mechanisms might influence their binding to ribosomes[63].

While cAMP and ppGpp have a predominant role in proteome allocation, additional regulatory mechanisms may become significant at very high levels of RelA induction. Zhu et al.[37] observed that when the growth rate is reduced from $\lambda = 0.9$ h^{-1} to $\lambda = 0.45$ h^{-1} by overexpressing RelA in glucose minimal medium, a stress response is triggered. Under such strong perturbations, our theoretical framework may break down, as cellular adaptations to growth slowdowns, which fall outside the scope of our present study, could influence the system. These include reorganization within the Q sector, potentially driven by global transcriptional coupling. However, these effects represent only a minor limitation, as our dataset covers a broad range of ppGpp concentrations, from physiological values to a few extreme overabundance points, with continuity. Moreover, proteomics data from Zhu et al. confirm that cAMP-activated genes are upregulated even under this strong perturbation (Fig. S4B). Further proteomics studies will be essential to explore the various regimes of ppGpp overabundance in more detail.

More widely, our findings show how the global effects of gene transcription should be understood within a framework of RNA polymerase allocation[29,30,72], much like the established proteome allocation model. Rather than viewing ppGpp as a direct regulator of ribosomal content, we show that its effects arise through global RNA polymerase redistribution, influenced by competition with other transcriptional programs. This perspective clarifies why changes in ppGpp levels alone do not fully predict ribosome synthesis and why conditions like ppGpp overabundance alter proteome composition in ways not captured by traditional promoter-centric models. This perspective may be widely applicable in understanding gene regulation.

RESOURCE AVAILABILITY

Lead contact

Requests for further information and resources should be directed to and will be fulfilled by the lead contact, Marco Cosentino Lagomarsino (marco.cosentino-lagomarsino@ifom.eu).

Data and code availability

- All original code and data are available on GitHub at this link.

ACKNOWLEDGMENTS

We thank Gabriele Micali, Luca Ciandrini, Bianca Sclavi, Philippe Fuchs, Martina Dal Bello and Paul Wiggins for useful discussions on this work. We thank Ferhat Büke, Marek Noga, Flora Yang, and Adja Zoumaro-Djayoon for technical assistance with ppGpp and cAMP quantification. The research leading to these results has received funding from AIRC under IG 2024 - ID. 30391 project – P.I. Marco Cosentino Lagomarsino. R.D. was supported by the AIRC fellowship Italy Pre-Doc 2022 (ID 28176). G.B. is supported by the Netherlands Organization for Scientific Research (NWO). M.L. was supported as part of the Frontiers of Nanoscience program.

AUTHOR CONTRIBUTIONS

Conceptualization, G.B. and M.C.L.; theoretical investigation, A.R. and R.D.; experiments, M.L.; data analysis, A.R., M.L., and R.D; writing A.R. and M.C.L.; funding acquisition, M.C.L., G.B., and R.D.; supervision, M.C.L. and G.B.

DECLARATION OF INTERESTS

The authors declare no competing interests.

DECLARATION OF GENERATIVE AI AND AI-ASSISTED TECHNOLOGIES

During the preparation of this work, the authors used ChatGPT for minor rephrasing of the text. After using this tool, the authors reviewed and edited the content as needed and take full responsibility for the content of the publication.

SUPPLEMENTAL INFORMATION INDEX

Note S1 and S2.

Table S1. Parameters obtained through fitting.

Figures S1-S5 and their legends.

Methods S1. Detailed information about modeling.

References

1. Scott, M., and Hwa, T. (2023). Shaping bacterial gene expression by physiological and proteome allocation constraints. Nature Reviews Microbiology *21*, 327–342. doi: 10.1038/s41579-022-00818-6. Epub 2022 Nov 14.

2. López-Maury, L., Marguerat, S., and Bähler, J. (2008). Tuning gene expression to changing environments: from rapid responses to evolutionary adaptation. Nature Reviews Genetics *9*, 583–593. doi: 10.1038/nrg2398.

3. Lee, T.I., and Young, R.A. (2013). Transcriptional regulation and its misregulation in disease. Cell *152*, 1237–1251. URL: https://www.sciencedirect.com/science/article/pii/S0092867413002031. doi: https://doi.org/10.1016/j.cell.2013.02.014.

4. Lo, T.W., Choi, H.J., Huang, D., and Wiggins, P.A. (2024). Noise robustness and metabolic load determine the principles of central dogma regulation. Science Advances *10*, eado3095. URL: https://www.science.org/doi/abs/10.1126/sciadv.ado3095. doi: 10.1126/sciadv.ado3095.

5. Hofmeyr, J.H.S., and Cornish-Bowden, A. (2000). Regulating the cellular economy of supply and demand. FEBS Letters *476*, 47–51. URL: https://febs.onlinelibrary.wiley.com/doi/abs/10.1016/S0014-5793%2800%2901668-9. doi: https://doi.org/10.1016/S0014-5793(00)01668-9.

6. Scott, M., Gunderson, C.W., Mateescu, E.M., Zhang, Z., and Hwa, T. (2010). Interdependence of cell growth and gene expression: Origins and consequences. Science *330*, 1099–1102. doi: 10.1126/science.1192588.

7. Scott, M., Klumpp, S., Mateescu, E.M., and Hwa, T. (2014). Emergence of robust growth laws from optimal regulation of ribosome synthesis. Molecular Systems Biology *10*, 747. URL: https://www.embopress.org/doi/abs/10.15252/msb.20145379. doi: https://doi.org/10.15252/msb.20145379.

8. Hui, S., Silverman, J.M., Chen, S.S., Erickson, D.W., Basan, M., Wang, J., Hwa, T., and Williamson, J.R. (2015). Quantitative proteomic analysis reveals a simple strategy of global resource allocation in bacteria. Mol Syst Biol *11*, 784. doi: 10.15252/msb.20145697.

9. Mori, M., Zhang, Z., Banaei-Esfahani, A., Lalanne, J., Okano, H., Collins, B., Schmidt, A., Schubert, O., Lee, D., Li, G., Aebersold, R., Hwa, T., and Ludwig, C. (2021). From coarse to fine: the absolute escherichia coli proteome under diverse growth conditions. Molecular Systems Biology *17*, e9536. doi: 10.15252/msb.20209536.

10. Zhu, M., and Dai, X. (2024). Shaping of microbial phenotypes by trade-offs. Nature Communications *15*, 4238. URL: https://doi.org/10.1038/s41467-024-48591-9. doi: 10.1038/s41467-024-48591-9.

11. Neidhardt, F.C., and Magasanik, B. (1960). Studies on the role of ribonucleic acid in the growth of bacteria. Biochimica et biophysica acta *42*, 99–116. URL: https://www.sciencedirect.com/science/article/pii/0006300260907575. Publisher: Elsevier.

12. Aebersold, R., and Mann, M. (2016). Mass-spectrometric exploration of proteome structure and function. Nature *537*, 347–355. doi: 10.1038/nature19949.

13. Beck, M., Schmidt, A., Malmstroem, J., Claassen, M., Ori, A., Szymborska, A., Herzog, F., Rinner, O., Ellenberg, J., and Aebersold, R. (2011). The quantitative proteome of a human cell line. Molecular Systems Biology *7*, 549. URL: https://www.embopress.org/doi/abs/10.1038/msb.2011.82. doi: https://doi.org/10.1038/msb.2011.82.

14. Metzl-Raz, E., Kafri, M., Yaakov, G., Soifer, I., Gurvich, Y., and Barkai, N. (2017). Principles of cellular resource allocation revealed by condition-dependent proteome profiling. eLife *6*, e28034. URL: https://doi.org/10.7554/eLife.28034. doi: 10.7554/eLife.28034.

15. Potrykus, K., Murphy, H., Philippe, N., and Cashel, M. (2011). ppgpp is the major source of growth rate control in e. coli. Environmental Microbiology *13*, 563–575. doi: 10.1111/j.1462-2920.2010.02357.x.

16. Barker, M.M., Gaal, T., Josaitis, C.A., and Gourse, R.L. (2001). Mechanism of regulation of transcription initiation by ppgpp. i. effects of ppgpp on transcription initiation in vivo and in vitro. Journal of Molecular Biology *305*, 673–688. doi: 10.1006/jmbi.2000.4327.

17. Lemke, J.J., Sanchez-Vazquez, P., Burgos, H.L., Hedberg, G., Ross, W., and Gourse, R.L. (2011). Direct regulation of escherichia coli ribosomal protein promoters by the transcription factors ppgpp and dksa. Proceedings of the National Academy of Sciences *108*, 5712–5717. URL: https://www.pnas.org/doi/abs/10.1073/pnas.1019383108. doi: 10.1073/pnas.1019383108.

18. Sanchez-Vazquez, P., Dewey, C.N., Kitten, N., Ross, W., and Gourse, R.L. (2019). Genome-wide effects on Escherichia coli transcription from ppgpp binding to its two sites on rna polymerase. Proceedings of the National Academy of Sciences *116*, 8310–8319. URL: https://www.pnas.org/doi/abs/10.1073/pnas.1819682116. doi: 10.1073/pnas.1819682116.

19. Wu, C., Balakrishnan, R., Braniff, N., Mori, M., Manzanarez, G., Zhang, Z., and Hwa, T. (2022). Cellular perception of growth rate and the mechanistic origin of bacterial growth law. Proceedings of the National Academy of Sciences *119*, e2201585119. doi: 10.1073/pnas.2201585119.

20. Irving, S.E., Choudhury, N.R., and Corrigan, R.M. (2021). The stringent response and physiological roles of (pp)pgpp in bacteria. Nature Reviews Microbiology *19*, 256–271. doi: https://doi.org/10.1038/s41579-020-00470-y.

21. Loveland, A.B., Bah, E., Madireddy, R., Zhang, Y., Brilot, A.F., Grigorieff, N., and Korostelev, A.A. (2016). Ribosome rela structures reveal the mechanism of stringent response activation. eLife *5*, e17029. URL: https://doi.org/10.7554/eLife.17029. doi: 10.7554/eLife.17029.

22. Arenz, S., Abdelshahid, M., Sohmen, D., Payoe, R., Starosta, A.L., Berninghausen, O., Hauryliuk, V., Beckmann, R., and Wilson, D.N. (2016). The stringent factor rela adopts an open conformation on the ribosome to stimulate ppgpp synthesis. Nucleic Acids Research *44*, 6471–6481. URL: https://doi.org/10.1093/nar/gkw470. doi: 10.1093/nar/gkw470.

23. Potrykus, K., and Cashel, M. (2008). (p)ppgpp: still magical? Annual Review of Microbiology *62*, 35–51. doi: 10.1146/annurev.micro.62.081307.162903.

24. Zhu, M., Pan, Y., and Dai, X. (2019). (p)ppgpp: the magic governor of bacterial growth economy. Curr Genet *65*, 1121–1125. URL: https://doi.org/10.1007/s00294-019-00973-z. doi: 10.1007/s00294-019-00973-z.

25. Mu, H., Han, F., Wang, Q., Wang, Y., Dai, X., and Zhu, M. (2023). Recent functional insights into the magic role of (p)ppgpp in growth control. Computational and Structural Biotechnology Journal *21*, 168–175. URL: https://www.sciencedirect.com/science/article/pii/S2001037022005578. doi: 10.1016/j.csbj.2022.11.063.

26. Lin, J., and Amir, A. (2018). Homeostasis of protein and mrna concentrations in growing cells. Nature Communications *9*, 4496. doi: 10.1038/s41467-018-06714-z.

27. Roy, A., Goberman, D., and Pugatch, R. (2021). A unifying autocatalytic network-based framework for bacterial growth laws. Proceedings of the National Academy of Sciences *118*, e2107829118. URL: https://www.pnas.org/doi/abs/10.1073/pnas.2107829118. doi: 10.1073/pnas.2107829118.

28. Calabrese, L., Ciandrini, L., and Cosentino Lagomarsino, M. (2024). How total mrna influences cell growth. Proceedings of the National Academy of Sciences *121*, e2400679121. URL: https://www.pnas.org/doi/abs/10.1073/pnas.2400679121. doi: 10.1073/pnas.2400679121.

29. Klumpp, S., Zhang, Z., and Hwa, T. (2009). Growth rate-dependent global effects on gene expression in bacteria. Cell *139*, 1366–1375. doi: 10.1016/j.cell.2009.12.001.

30. Balakrishnan, R., Mori, M., Segota, I., Zhang, Z., Aebersold, R., Ludwig, C., and Hwa, T. (2022). Principles of gene regulation quantitatively connect dna to rna and proteins in bacteria. Science *378*, eabk2066. doi: 10.1126/science.abk2066.

31. Fic, E., Bonarek, P., Gorecki, A., Kedracka-Krok, S., Mikolajczak, J., Polit, A., Tworzydlo, M., Dziedzicka-Wasylewska, M., and Wasylewski, Z. (2008). cAMP Receptor Protein from Escherichia coli as a Model of Signal Transduction in Proteins – A Review. Journal of Molecular Microbiology and Biotechnology *17*, 1–11. URL: https://doi.org/10.1159/000178014. doi: 10.1159/000178014.

32. You, C., Okano, H., Hui, S., Zhang, Z., Kim, M., Gunderson, C., Wang, Y., P., L., Yan, D., and Hwa, T. (2013). Coordination of bacterial proteome with metabolism by cyclic AMP signalling. Nature *500*, 301–306. doi: 10.1038/nature12446.

33. Towbin, B.D., Korem, Y., Bren, A., Doron, S., Sorek, R., and Alon, U. (2017). Optimality and sub-optimality in a bacterial growth law. Nature Communications *8*, 14123. URL: https://doi.org/10.1038/ncomms14123. doi: 10.1038/ncomms14123.

34. Droghetti, R., Fuchs, P., Iuliani, I., Firmano, V., Tallarico, G., Calabrese, L., Grilli, J., Sclavi, B., Ciandrini, L., and Cosentino Lagomarsino, M. (2025). Incoherent feedback from coupled amino acids and ribosome pools generates damped oscillations in growing e. coli. Nature Communications *16*. URL: http://dx.doi.org/10.1038/s41467-025-57789-4. doi: 10.1038/s41467-025-57789-4.

35. Zhu, M., and Dai, X. (2019). Growth suppression by altered (p)ppgpp levels results from non-optimal resource allocation in escherichia coli. Nucleic Acids Research *47*, 4684–4693. doi: 10.1093/nar/gkz211.

36. Zhu, M., and Dai, X. (2023). Stringent response ensures the timely adaptation of bacterial growth to nutrient downshift. Nature Communications *14*, 467. doi: 10.1038/s41467-023-36254-0.

37. Zhu, M., Mu, H., and Dai, X. (2024). Integrated control of bacterial growth and stress response by (p)ppgpp in Escherichia coli: A seesaw fashion. iScience *27*, 108818. doi: 10.1016/j.isci.2024.108818.

38. Kochanowski, K., Okano, H., Patsalo, V., Williamson, J., Sauer, U., and Hwa, T. (2021). Global coordination of metabolic pathways in escherichia coli by active and passive regulation. Molecular Systems Biology *17*, e10064. doi: 10.15252/msb.202010064.

39. Schreiber, G., Metzger, S., Aizenman, E., Roza, S., Cashel, M., and Glaser, G. (1991). Overexpression of the rela gene in Escherichia coli. Journal of Biological Chemistry *266*, 3760–3767.

40. Noga, M.J., Büke, F., van den Broek, N.J.F., Imholz, N.C.E., Scherer, N., Yang, F., and Bokinsky, G. (2020). Posttranslational control of plsb is sufficient to coordinate membrane synthesis with growth in escherichia coli. mBio *11*, 10.1128/mbio.02703–19. URL: https://journals.asm.org/doi/abs/10.1128/mbio.02703-19. doi: 10.1128/mbio.02703-19.

41. Spira, B., and Ospino, K. (2020). Diversity in e. coli (p)ppgpp levels and its consequences. Frontiers in Microbiology *11*. URL: http://dx.doi.org/10.3389/fmicb.2020.01759. doi: 10.3389/fmicb.2020.01759.

42. Imholz, N., Noga, M., van den Broek, N., and Bokinsky, G. (2020). Calibrating the bacterial growth rate speedometer: A re-evaluation of the relationship between basal ppgpp, growth, and rna synthesis in escherichia coli. Frontiers in Microbiology *11*, 574872. doi: 10.3389/fmicb.2020.574872.

43. Bosdriesz, E., Molenaar, D., Teusink, B., and Bruggeman, F.J. (2015). How fast-growing bacteria robustly tune their ribosome concentration to approximate growth-rate maximization. FEBS Journal *282*, 2029–2044. doi: 10.1111/febs.13258.

44. Chure, G., and Cremer, J. (2023). An optimal regulation of fluxes dictates microbial growth in and out of steady state. eLife *12*, e84878. URL: https://doi.org/10.7554/eLife.84878. doi: 10.7554/eLife.84878.

45. Dai, X., Zhu, M., Warren, M., Balakrishnan, R., Patsalo, V., Okano, H., Williamson, J.R., Fredrick, K., Wang, Y.P., and Hwa, T. (2016). Reduction of translating ribosomes enables *Escherichia coli* to maintain elongation rates during slow growth. Nature Microbiology *2*, 16231. doi: 10.1038/nmicrobiol.2016.231.

46. Calabrese, L., Grilli, J., Osella, M., Kempes, C.P., Cosentino Lagomarsino, M., and Ciandrini, L. (2022). Protein degradation sets the fraction of active ribosomes at vanishing growth. PLoS Comput Biol *18*, e1010059. doi: 10.1371/journal.pcbi.1010059.

47. Klumpp, S., and Hwa, T. (2014). Bacterial growth: global effects on gene expression, growth feedback and proteome partition. Current Opinion in Biotechnology *28*, 96–102. doi: 10.1016/j.copbio.2014.01.001. Epub 2014 Feb 2.

48. Hauryliuk, V., Atkinson, G., Murakami, K., Tenson, T., and Gerdes, K. (2015). Recent functional insights into the role of (p)ppgpp in bacterial physiology. Nature Reviews Microbiology *13*, 298–309. doi: 10.1038/nrmicro3448.

49. Zhu, M., Mori, M., Hwa, T., and Dai, X. (2019). Disruption of transcription-translation coordination in escherichia coli leads to premature transcriptional termination. Nature Microbiology *4*, 2347–2356. doi: 10.1038/s41564-019-0543-1. Epub 2019 Aug 26.

50. Erickson, D., Schink, S., Patsalo, V., Williamson, J., Gerland, U., and Hwa, T. (2017). A global resource allocation strategy governs growth transition kinetics of escherichia coli. Nature *551*, 119–123. doi: 10.1038/nature24299.

51. Okano, H., Hermsen, R., Kochanowski, K., and Hwa, T. (2020). Regulation underlying hierarchical and simultaneous utilization of carbon substrates by flux sensors in escherichia coli. Nature Microbiology *5*, 206–215. doi: 10.1038/s41564-019-0610-7. Epub 2019 Dec 9.

52. Wehrens, M., Krah, L.H., Towbin, B.D., Hermsen, R., and Tans, S.J. (2023). The interplay between metabolic stochasticity and camp-crp regulation in single *E. coli* cells. Cell Reports *42*, 113284. URL: https://doi.org/10.1016/j.celrep.2023.113284. doi: 10.1016/j.celrep.2023.113284.

53. Botsford, J.L., and Harman, J.G. (1992). Cyclic amp in prokaryotes. Microbiology Reviews *56*, 100–122. doi: 10.1128/mr.56.1.100-122.1992.

54. Kochanowski, K., Gerosa, L., Brunner, S.F., Christodoulou, D., Nikolaev, Y.V., and Sauer, U. (2017). Few regulatory metabolites coordinate expression of central metabolic genes in escherichia coli. Molecular Systems Biology *13*, 903. doi: 10.15252/msb.20167402.

55. Büke, F., Grilli, J., Cosentino Lagomarsino, M., Bokinsky, G., and Tans, S. (2022). ppgpp is a bacterial cell size regulator. Current Biology *32*, 870–877.e5. URL: https://doi.org/10.1016/j.celrep.2022.02.023. doi: 10.1016/j.celrep.2022.02.023.

56. Duysak, T., Tran, T.T., Afzal, A.R., and Jung, C.H. (2021). Fluorescence spectroscopic analysis of ppgpp binding to camp receptor protein and histone-like nucleoid structuring protein. International Journal of Molecular Sciences *22*, 7871. URL: https://doi.org/10.3390/ijms22157871. doi: 10.3390/ijms22157871.

57. Fernández-Coll, L., Maciag-Dorszynska, M., Tailor, K., Vadia, S., Levin, P.A., Szalewska-Palasz, A., and Cashel, M. (2020). The absence of (p)ppgpp renders initiation of escherichia coli chromosomal dna synthesis independent of growth rates. mBio *11*, e03223–19. doi: 10.1128/mBio.03223-19.

58. Paul, B.J., Barker, M.M., Ross, W., Schneider, D.A., Webb, C., Foster, J.W., and Gourse, R.L. (2004). Dksa: A critical component of the transcription initiation machinery that potentiates the regulation of rrna promoters by ppgpp and the initiating ntp. Cell *118*, 311–322. URL: https://doi.org/10.1016/j.cell.2004.07.009. doi: 10.1016/j.cell.2004.07.009. Doi: 10.1016/j.cell.2004.07.009.

59. Chandrangsu, P., Lemke, J.J., and Gourse, R.L. (2011). The dksa promoter is negatively feedback regulated by dksa and ppgpp. Molecular Microbiology *80*, 1337–1348. doi: 10.1111/j.1365-2958.2011.07649.x. Epub 2011 Apr 17.

60. Svitil, A.L., Cashel, M., and Zyskind, J.W. (1993). Guanosine tetraphosphate inhibits protein synthesis in vivo. a possible protective mechanism for starvation stress in *Escherichia coli*. J Biol Chem *268*, 2307–2311.

61. Polikanov, Y.S., Blaha, G.M., and Steitz, T.A. (2012). How hibernation factors rmf, hpf, and yfia turn off protein synthesis. Science *336*, 915–918. doi: 10.1126/science.1218538.

62. Häuser, R., Pech, M., Kijek, J., Yamamoto, H., Titz, B., Naeve, F., Tovchigrechko, A., Yamamoto, K., Szaflarski, W., Takeuchi, N., Stellberger, T., Diefenbacher, M.E., Nierhaus, K.H., and Uetz, P. (2012). Rsfa (ybeb) proteins are conserved ribosomal silencing factors. PLoS Genetics *8*, e1002815. doi: 10.1371/journal.pgen.1002815.

63. Maki, Y., and Yoshida, H. (2021). Ribosomal hibernation-associated factors in escherichia coli. Microorganisms *10*, 33. doi: 10.3390/microorganisms10010033.

64. Shimada, T., Yoshida, H., and Ishihama, A. (2013). Involvement of cyclic amp receptor protein in regulation of the rmf gene encoding the ribosome modulation factor in escherichia coli. Journal of Bacteriology *195*, 2212–2219. doi: 10.1128/JB.02279-12. Epub 2013 Mar 8.

65. Guo, Y., and Amir, A. (2021). Exploring the effect of network topology, mrna and protein dynamics on gene regulatory network stability. Nature Communications *12*, 130. URL: https://doi.org/10.1038/s41467-020-20472-x. doi: 10.1038/s41467-020-20472-x.

66. Lempp, M., Farke, N., Kuntz, M., Freibert, S.A., Lill, R., and Link, H. (2019). Systematic identification of metabolites controlling gene expression in *E. coli*. Nature Communications *10*, 4463. URL: https://doi.org/10.1038/s41467-019-12474-1. doi: 10.1038/s41467-019-12474-1.

67. Ro, C., Cashel, M., and Fernández-Coll, L. (2021). The secondary messenger ppgpp interferes with camp-crp regulon by promoting crp acetylation in *Escherichia coli*. PLoS One *16*, e0259067. doi: 10.1371/journal.pone.0259067.

68. Zhao, L., Zhou, S.Y., Fu, Y. et al. (2024). A dual program for crp-mediated regulation in bacterial alarmone (p)ppgpp. mBio *15*, e0243024. doi: 10.1128/mbio.02430-24.

69. Salgado, H., Gama-Castro, S., Lara, P., Mejia-Almonte, C., Alarcón-Carranza, G., López-Almazo, A.G., Betancourt-Figueroa, F., Peña-Loredo, P., Alquicira-Hernández, S., Ledezma-Tejeida, D. et al. (2023). Regulondb v12.0: a comprehensive resource of transcriptional regulation in e. coli k-12. Nucleic Acids Research *52*, D255–D264. URL: https://doi.org/10.1093/nar/gkad1072. doi: 10.1093/nar/gkad1072.

70. Moore, L., Caspi, R., Boyd, D., Berkmen, M., Mackie, A., Paley, S., and Karp, P. (2024). Revisiting the y-ome of escherichia coli. Nucleic Acids Research *52*, 12201–12207. URL: https://doi.org/10.1093/nar/gkae857. doi: 10.1093/nar/gkae857.

71. Melamed, S., Peer, A., Faigenbaum-Romm, R., Gatt, Y.E., Reiss, N., Bar, A., Altuvia, Y., Argaman, L., and Margalit, H. (2016). Global mapping of small rna-target interactions in bacteria. Molecular Cell *63*, 884–897. URL: https://www.sciencedirect.com/science/article/pii/S1097276516304130. doi: https://doi.org/10.1016/j.molcel.2016.07.026.

72. Zhang, Q., Brambilla, E., Li, R., Shi, H., Cosentino Lagomarsino, M., and Sclavi, B. (2020). A decrease in transcription capacity limits growth rate upon translation inhibition. mSystems *5*, 10.1128/msystems.00575–20. URL: https://journals.asm.org/doi/abs/10.1128/msystems.00575-20. doi: 10.1128/msystems.00575-20.

73. Cooper, S., and Helmstetter, C.E. (1968). Chromosome replication and the division cycle of escherichia coli. Br. J. Mol. Biol. *31*, 519–540. doi: 10.1016/0022-2836(68)90425-7.

74. Bremer, H., and Churchward, G. (1977). An examination of the cooper-helmstetter theory of dna replication in bacteria and its underlying assumptions. Journal of Theoretical Biology *69*, 645–654. URL: https://www.sciencedirect.com/science/article/pii/0022519377903733. doi: https://doi.org/10.1016/0022-5193(77)90373-3.

75. Bachmann, B.J. (1990). Linkage map of Escherichia coli k-12, edition 8. Microbiological Reviews *54*, 130–197. doi: 10.1128/mr.54.2.130-197.1990. Erratum in: Microbiol Rev 1991 Mar;55(1):191.

STAR METHODS

Experimental model details

In this study, we used the wild type E. coli NCM3722 K-12 strain and its derivative RelA* overexpression strain. For all the experiments, cultures were inoculated directly from a single colony of the desired strain from a LB agar plate.

The RelA* overexpression strain is the same as the one described in Noga *et al.*[40] (pSC101-kanR-TetR RelA*-mVenus), where RelA* can be induced by doxycycline.

Method details

Media

In all experiments bacterial cultures were grown in MOPS minimal medium, using 15N isotope NH4Cl as nitrogen source supplemented with 2% carbon source, which could be glucose, succinate, glycerol, acetate, aspartate or glutamate. The two carbon sources containing nitrogen were also 15N isotopes.

Growth Protocol

Optical density at 600nm was monitored every 5sec to 1min using regular measurements of culture turbidity by an automated absorbance measurement system. Briefly, liquid culture is constantly pumped through a flow through cuvette, measured for optical density at frequent intervals and subsequently pumped back into the flask. Growth rate is extracted by smoothing OD measurements with a 5 minute wide gaussian filter on OD measurements and taking median of the time derivative of the neperian logarithm on a one hour window for precise determination of steady state growth rates.

ppGpp and cAMP measurements

Nucleotide concentrations were quantified using a tandem liquid chromatography mass spectrometry (LC-MS) methodology slightly adapted from ref.[40] (higher sampling volume and repeated washing steps to be able efficiently measure low concentrations). Briefly, samples were taken at 0.35 OD after growth rate stabilized (usually 3 to 5 hours after inducing RelA*), filtered, quenched in formic acid, pelleted and frozen at -80℃. For analysis, frozen samples were thawed and purified.

Quantification and statistical analysis

Quantification of ppGpp and cAMP concentration

For both ppGpp and cAMP, 14N and 15N peaks, corresponding respectively to standard concentration added and biological sample, were obtained through LC-MS. The concentrations shown

in Fig. 2,3,4, 5 expressed in pmol/OD600 were obtained by multiplying the 15N/14N area ratio by the added compound concentration, then normalizing by OD600 at sampling. The OD600 value was determined as the average of the last measurement before sampling and the first measurement after sampling. Error bars represent standard errors reflecting variability across technical replicates.

Conversion of growth rates into ribosomal fractions and elongation rates

To convert our growth rate data (Fig S1) into ribosomal fractions, we applied a linear fit to the total RNA/protein ratio measurements r from Zhu et al.[35], leveraging the conservation of the ribosomal growth law (Fig S2A):

$$r(\lambda) = q + m\lambda \ , \tag{15}$$

with $q = 0.073$ and $m = 0.217\ h$. We note that interpolating data from Dai et al.[45] yields substantially the same coefficients q and m. To obtain the "extended" ribosomal fraction, we then transformed RNA/protein ratios with the following conversion:

$$\phi_R = z \cdot r, \tag{16}$$

with $z = 0.76$, as discussed in Scott et al.[6].

To convert our growth rate data into elongation rate values, we leveraged the conservation of the elongation rate growth law under RelA overexpression[35] (Fig.S2B) and computed

$$\epsilon = \epsilon_{max} \frac{r(\lambda)}{r(\lambda) + k_M}, \tag{17}$$

with $\epsilon_{max} = 6.44\ h^{-1}$ (equivalent to 22 amino acids/s, see Methods S1) and $k_M = 0.11$ as in Dai et al.[45]. Note that Fig. 4 is independent of the value we choose for ϵ_{max}, as only the ratio $\frac{\epsilon_{max}}{\epsilon}$ appears in the definition of the x-axis.

The knowledge of the relationships $\epsilon(\lambda)$ and $\phi_R(\lambda)$ allows us to compute $f_a = \frac{\lambda}{\epsilon\phi_R}$ for each data point in this study.

Generating the wild-type active ribosomes-ppGpp curve (Fig. 5)

To generate the wild-type gray curves in Fig. 5B and Fig. 5C, we first fitted a linear relationship between ϕ_R and ppGpp (following ref.[19]), $\phi_R = c_0 \frac{1}{g}$, as in Fig. 2B. The quantities λ and ϵ can be obtained from ϕ_R by inverting the relationships (15), (16) and (17) found in the previous paragraph. This allows us to express $f_a = \frac{\lambda}{\epsilon\phi_R}$ as a function of ppGpp (Fig. 5B). The wild-type curve in Fig. 5C can be computed from f_a and ϕ_R through the relation $\phi_R^{in} = \phi_R(1 - f_a)$.

Modeling - coarse grained promoter strengths

To define the coarse-grained sector strengths in equation (5), we start from (3), and sum over the genes belonging to the same sector, leading to the coarse-grained messenger dynamics

$$\frac{d[m_I]}{dt} = \sum_{j \in I} k_j(\{r\})[G_j][N_{av}] - (\delta + \lambda)[m_I] \ . \tag{18}$$

We define the coarse-grained "sector strengths", as

$$\beta_I := \sum_{j \in I} k_j \ , \tag{19}$$

which gives (5) if all genes are assumed to be present at the same concentration $[G]$.

Modeling - gene dosage effects

To incorporate gene dosage effects in our model, we express gene concentrations relative to the origin of replication (Ori), $[G_i] = d_i(\lambda, x_i)[Ori]$, with the dose d_i depending on the normalized distance x_i between gene and Ori, with the replication terminus (Ter) corresponding to $x = 1$[30,73,74]. For each sector, we can define a "regulatory activity", consistently with the terminology of Balakrishnan *et al.*.[30], as

$$\theta_I := \sum_{j \in I} k_j(\{r\}) d_j(x_j, \lambda) \ . \tag{20}$$

Using this definition, we obtain an equation describing the transcripts dynamics for each sector,

$$\frac{d[m_I]}{dt} = \theta_I [Ori][N_{av}] - (\delta + \lambda)[m_I], \tag{21}$$

which incorporates both transcription factor regulation and gene dosage effects.

In fast growth conditions, the relative abundance of genes located near the origin of replication tends to increase, enhancing the expression of certain genes, such as those encoding ribosomal proteins and ribosomal RNA[75]. To include this in our model, we use a mean-field approximation by assigning each gene in a given sector to a single chromosomal position x_I, thus writing $\theta_I = d(x_I, \lambda) \sum_{j \in I} k_j$. To obtain the parameters in Table 1, we set $x_R = 0.25$, and $x_P = 0.6$, reflecting the advantage at fast growth for ribosomal genes (see Methods S1 for details on how these values were estimated). This approximation leads to the factorization

$$\theta_I = \beta_I d(x_I, \lambda) \ , \tag{22}$$

which separates the influence of transcription factors from gene dosage effects. With this setting, one still finds (6), but with the definition

$$\omega_I := \frac{\theta_I}{\sum_J \theta_J} \ . \tag{23}$$

Methods S1 provides the full mathematical formulation of the model variant that includes gene dosage effects, which we used to replicate the data analyses and parameter fitting described in the main text. As already described by Balakrishnan *et al.*[30], gene dosage effects are small in the range of conditions explored in this study ($0.2 - 1\ h^{-1}$). This model variant can be mapped onto the simplified version used in the main text by assuming the same gene copy number for all sectors (e.g., by setting $x_I = 0.5$ for all I). This leads to:

$$\omega_I = \frac{\theta_I}{\sum_J \theta_J} = \frac{\beta_I}{\sum_J \beta_J} \ , \tag{24}$$

which then gives (7) in the steady state.

Fitting the model of transcriptional competition to ribosomal fractions

Data fitting of ribosomal fractions was performed through Orthogonal Distance Regression. A detailed explanation of the fitting approach can be found in Methods S1. Although we did not perform comparative modeling, we can assess the goodness of fit for our model in Fig. 3A by calculating a coefficient of determination. Specifically, we compared a linear model that uses our growth rate prediction (based on ppGpp and cAMP concentrations for each condition as inputs)

as the explanatory variable against the measured growth rate. The results are shown in Table 1, and visualized in Fig. S3A for the model used in the main text (without gene dosage effects).

Transcriptional competition theory for hibernation factors

To explain the deviations in f_a as a function of ppGpp (Fig. 5), we focused on ribosome hibernation factors. We group these factors into a new sector characterized by a mass fraction ϕ_{HIB} and a regulatory activity θ_{HIB}. We assume that hibernation factors are in competition with P and R, and use the same ϕ_Q and ϕ_{max} of the three sector model: equation 7 for the hibernation sector reads

$$\omega_{HIB} = \frac{\theta_{HIB}}{\theta_{TOT}} = \frac{\theta_{HIB}}{\theta_R + \theta_P + \theta_{HIB}}\phi_{max} \approx \frac{\theta_{HIB}}{\theta_R + \theta_P}\phi_{max}, \tag{25}$$

where we neglect the term θ_{HIB} at the denominator given the small size of the hibernation sector, based on the proteomics data in ref.[9]. At steady-state $\omega_{HIB} = \phi_{HIB}$ due to (7), and ignoring gene dosage effects, we find from the above equation

$$\phi_{HIB} = \frac{\beta_{HIB}(\cdot)}{\beta_R(g) + \beta_P(c)}\phi_{max}.$$

Specializing this equation to points A and B in Fig. 5D leads to (14) of the main text.